ACS APPLIED MATERIALS & INTERFACES

Letter

www.acsami.org

Highly Efficient Layer-by-Layer-Assisted Infiltration for High-Performance and Cost-Effective Fabrication of Nanoelectrodes

Yuri Choi,[†,‡] Sihyuk Choi,[†,‡] Hu Young Jeong,[§] Meilin Liu,[‡,⊥] Byeong-Su Kim,*[,‡,#] and Guntae Kim*[,‡]

[‡]Department of Energy Engineering, [§]UNIST Central Research Facilities (UCRF), Department of Mechanical and Advanced Materials Engineering, and [#]Department of Chemistry, Ulsan National Institute of Science and Technology (UNIST), Ulsan 689-798, Korea

[⊥]School of Material Science and Engineering, Georgia Institute of Technology, Atlanta, Georgia 30332, United States

Supporting Information

ABSTRACT: We present a novel cathode fabrication technique for improved performance and production efficiency of SOFCs based on an infiltration method assisted by layer-by-layer (LbL) assembly of polyelectrolytes. Preparation of the electrode with LbL-assisted infiltration leads to a 6.5-fold reduction in the electrode fabrication time while providing uniform and small formation of $Pr_{0.7}Sr_{0.3}CoO_{3-\delta}$ (PSC) particles on the electrode. The increased surface area by 24.5% and number of active sites of the prepared electrode exhibits superior electrochemical performance up to 36.1% while preserving the electrical properties of the electrode. Because of its versatility and tenability, the LbL-assisted infiltration process may become a new route for fabrication of composite electrodes for other energy storage and conversion devices.

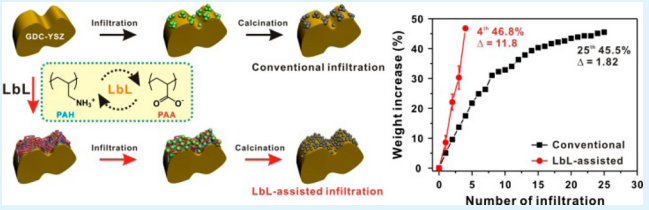

KEYWORDS: *layer-by-layer assembly, solid oxide fuel cell (SOFC), infiltration, composite electrode, oxygen reduction reaction*

Solid oxide fuel cells (SOFCs) are considered promising electrochemical devices for direct conversion of chemical energy to electricity with high efficiency, high power density, low emission, and excellent fuel flexibility.[1,2] However, commercialization of SOFC technologies is hindered by the high cost and the problems associated with the high operating temperature of SOFCs (>800 °C), including degradation of cell components because of corrosion, interdiffusion, and structural failure. To overcome these issues, the operating temperature must be significantly reduced. Unfortunately, however, the polarization loss at the cathode increases rapidly as the working temperature is lowered, leading to dramatically reduced fuel cell performance.[3,4] The development of appropriate cathode materials with high electrocatalytic activity for oxygen reduction reaction (ORR) at lower temperatures is thus considered imperative.[5,6] In addition, the development of a new process for cost-effective fabrication of electrodes with controlled microstructures is critical to improving both ionic and electronic conductivity and catalytic activity at lower operating temperatures.

The conventional approach to fabrication of composite electrodes involves the deposition of a mixture of electrolyte and electrode material (such as screen printing and spin coating) followed by high-temperature sintering. The undesired reactions between the electrode and electrolyte materials at high temperatures often impose restrictions on the choice of materials and processing conditions, greatly limiting the composition and microstructure and thus the properties of electrodes.[7,8] In order to avoid these difficulties as well as to separate the sintering of the electrolyte (at high temperatures) from the firing of the other electrode components (at lower temperatures), infiltration has recently been used for fabrication of composite electrodes.[9−12] Infiltration is very flexible, allowing the use of a wide range of anode and cathode compositions. For example, a porous yttria-stabilized zirconia (YSZ) scaffold is first co-sintered with a dense YSZ electrolyte membrane. Then, the precursor solution of an electrode material is coated on the surface of the porous YSZ by a solution infiltration process.[10,11,13−15] This method produces electrodes with longer triple-phase-boundaries (TPBs, or the electrochemical reactive sites), thereby enhancing the performance of the composite electrode. Furthermore, such a composite electrode has a uniform structure because a conducting phase is added to the existing YSZ backbone, leading to enhanced conductivity.[16,17]

However, it is necessary to load sufficient amounts of electronically conductive materials to the scaffold in order to maintain efficient current collection and minimize sheet resistance. Thus, repeated cycles of infiltration are often required (typically more than 50 cycles), which could be tedious and costly for implementation, especially for commercialization. To overcome this critical challenge, here we report a novel fabrication process: infiltration assisted by layer-by-layer (LbL) assembly. Specifically, we employed an LbL assembled polyelectrolyte multilayer film on the YSZ electrolyte scaffold as a matrix to guide the infiltration of

Received: July 24, 2014
Accepted: October 6, 2014
Published: October 6, 2014

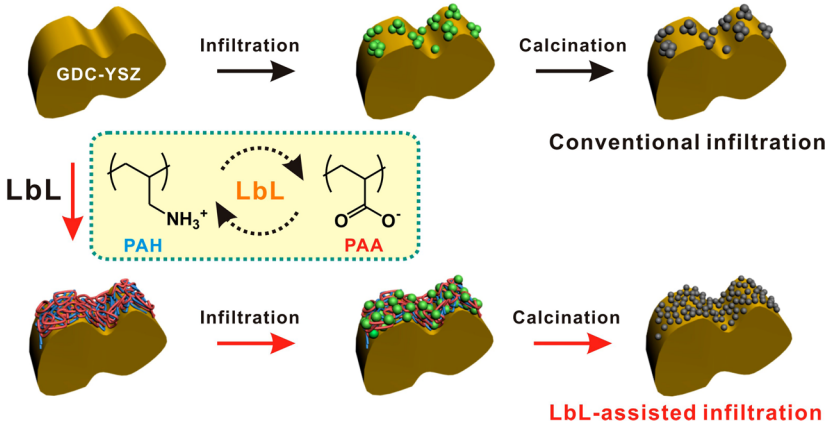

Figure 1. Schematic representation of (top) conventional infiltration method and (bottom) layer-by-layer (LbL) assembled polyelectrolyte multilayer-assisted infiltration for a SOFC electrode.

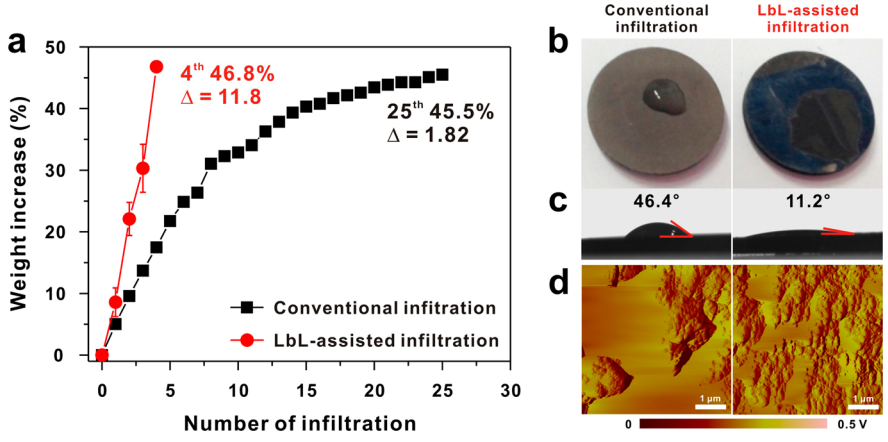

Figure 2. (a) Weight changes of a single cell with the number of infiltration cycles. (b–d) Comparison of (left) conventional infiltration and (right) LbL-assisted infiltration. (b) Optical images after dropping 5 μL of water onto a plain PSC substrate, (c) corresponding contact angle images, and (d) AFM images after calcination clearly depicting the more uniform coating obtained with the LbL-assisted infiltration method due to enhanced wetting on PSC.

precursor materials, significantly reducing the number of repeated cycles of infiltration required to complete the deposition. The electrode fabricated by this novel LbL-assisted infiltration method has a conformal coating of the active electrode materials on the surface of the scaffolds with high performance.

LbL assembly has been widely used as a versatile method for fabricating multilayer thin films onto solid surfaces with controlled structure and composition.[18−21] It is typically based on sequential adsorption of materials with complementary functional groups employing electrostatic interactions, hydrogen bonding, or covalent interactions. Because of their facile, inexpensive, and environmentally friendly nature, LbL assembled multilayer thin films have found broad applications, ranging from energy and electrochemical devices to biomedical materials.[22−24] In particular, recent advances in LbL-based nanostructured electrode formation include direct integration of active materials into the electrode, surface modification with polyionic salts into charged multilayers, and the use of metal complexed polymer electrolytes.[25−29] However, here we employed the polyelectrolyte multilayer formation followed by infiltration with metal precursors, and to the best of our knowledge, this is the first report of employing a LbL assembly in the fabrication of a SOFC electrode.

The LbL-assembled polyelectrolyte multilayer on a $Gd_{0.1}Ce_{0.9}O_{2-\delta}$ (GDC)-YSZ electrolyte substrate was prepared by sequential LbL assembly between positively charged poly(allylamine hydrochloride) (PAH) and negatively charged poly(acrylic acid) (PAA), as illustrated in Figure 1. As-prepared GDC-YSZ was alternately immersed in aqueous solutions of PAH and PAA at pH 3, with extensive water rinsing between each deposition. After finishing the LbL assembly process for the creation of thin multilayer films of PAH/PAA, a precursor solution of $Pr_{0.7}Sr_{0.3}CoO_{3-\delta}$ (PSC) was infiltrated onto the LbL-multilayer coated YSZ and metal ions were intercalated into the polyelectrolyte multilayer. Subsequently, the YSZ substrate underwent calcination in air at 450 °C to decompose the polyelectrolyte multilayers and nitrate ions. The whole process was repeated until the final loading reached 45 wt %, and the composite was finally fired at 850 °C in air for 4 h to form the desired perovskite structure. A control experiment using the conventional infiltration method was performed under identical reaction conditions without the use of LbL assembly on a GDC-YSZ electrolyte substrate.

Figure 2a shows the weight changes of a single cell with the number of infiltration cycles of conventional and LbL-assisted infiltration, respectively. The time necessary for LbL-assisted infiltration is significantly shorter than that of the conventional infiltration, by a factor of 6.5 times (11.8 wt % vs 1.82 wt %

dx.doi.org/10.1021/am5048834 | ACS Appl. Mater. Interfaces 2014, 6, 17352−17357

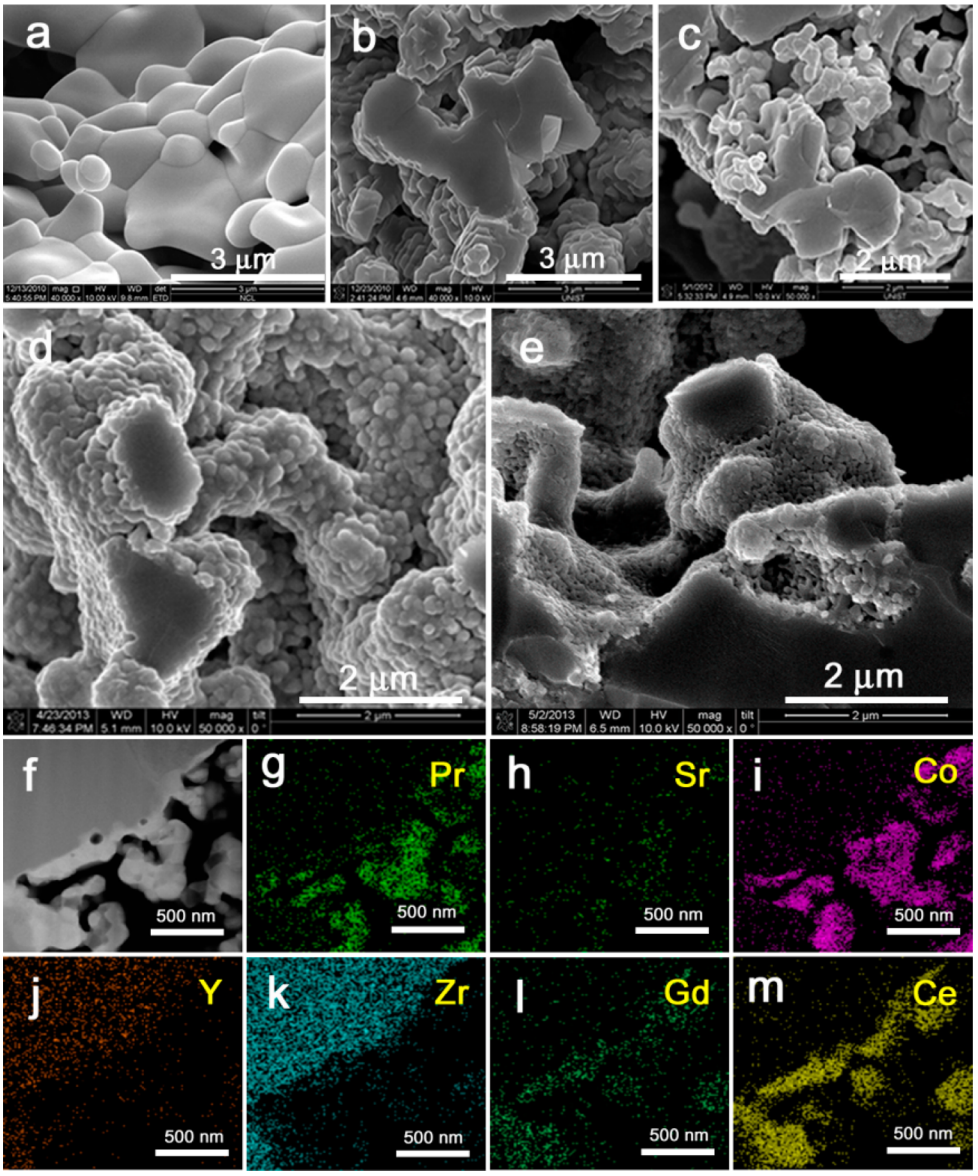

Figure 3. SEM images of (a) plain YSZ scaffold, (b) GDC-YSZ composites with 15 wt % GDC sintered at 1200 °C, (c) LbL treated GDC-YSZ, (d) conventional infiltrated PSC, and (e) LbL-assisted infiltrated PSC. Energy-dispersive spectroscopy (EDS) spectrum and elemental mapping of the PSC-YSZ sintered at 850 °C. (f) Scanning TEM (STEM) high-angle annular dark-field (HAADF) image and (g–m) elemental mapping of Pr, Sr, Co, Y, Zr, Gd, and Ce, respectively.

loading per cycle). As expected, metal ions are well intercalated into the polyelectrolyte multilayer in a single infiltration step and large amounts of PSC particles can coat the porous structure of the substrate after the calcination process. To prove that the reduced processing time is due to the enhanced surface wetting effects, we performed a water drop test and contact angle measurement (Figure 2b, c). The surface of the GDC-YSZ becomes considerably more hydrophilic after the LbL assembly step, which clearly demonstrates that the polyelectrolyte multilayer enhances the wettability of the matrix with regard to the infiltration solution, similar to typical LbL assembly reported previously.[30] Additionally, these results confirm that the LbL assembly facilitates the adsorption and formation of PSC particles in porous GDC-YSZ during infiltration and calcination. We found that other polyelectrolyte multilayers such as a multilayer composed of poly(dimethyldiallyl ammonium chloride) and poly(styrene 4-sulfonate) also assisted in loading PSC particles onto GDC-YSZ with significantly fewer infiltration cycles than required in the conventional method (see Figure S1 in the Supporting Information).

Atomic force microscopy (AFM) images and line scan profiles further support the differences in morphologies of each substrate after the deposition of PSC nanoparticles (Figure 2d). As a model system, we employed a flat PSC substrate, as particle growth mainly occurs on the surface of PSC after the initial deposition on the GDC-YSZ layer. As demonstrated in the AFM images, PSC particles partially covered the PSC substrate in the case of conventional infiltration, whereas metal nanoparticles uniformly cover a large fraction of PSC in the case of LbL-assisted infiltration. Surface root-mean-square roughness (R_{rms}) values of conventional and LbL-assisted infiltration are determined to be 64.7 and 42.3 nm, respectively. The reduced surface roughness is ascribed to the uniform and

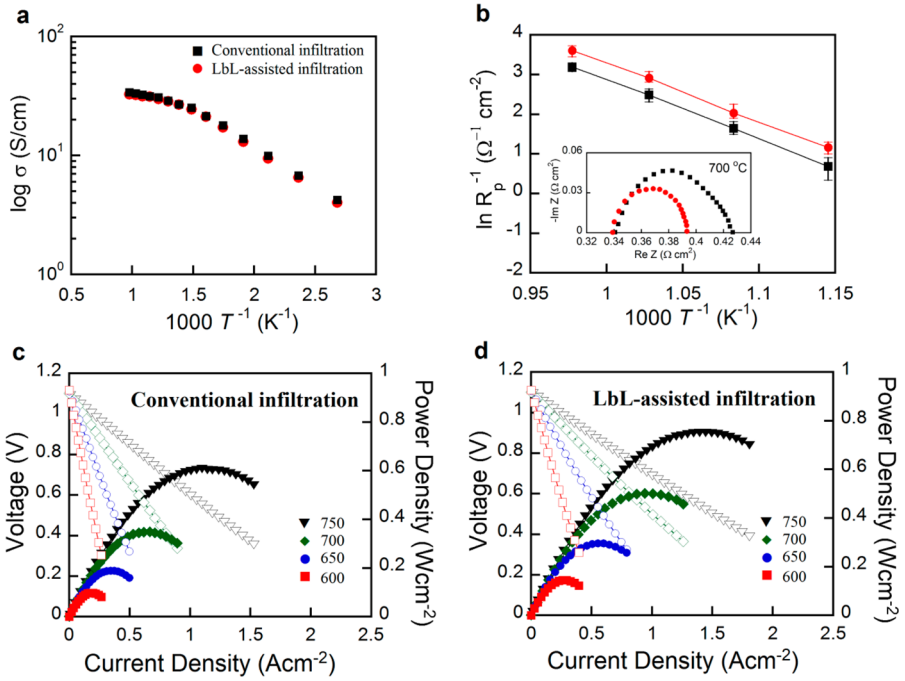

Figure 4. (a) Electrical conductivity of PSC-GDC-YSZ infiltrated on bare YSZ (black square) and on LbL treated YSZ (red circle) in air. (b) Arrhenius plot of reciprocal area specific resistance (ASR) of PSC-GDC-YSZ composite prepared by each infiltration method. The inset shows the ASR of the PSC-GDC-YSZ cathode with conventional (black square) and LbL-assisted method (red circle) measured at 700 °C in air under open-circuit conditions. *I*–*V* curves and the corresponding power densities of test cells with a PSC-GDC-YSZ cathode by (c) conventional infiltration and (d) LbL-assisted infiltration using humidified H_2 (3% H_2O) as the fuel and ambient air as the oxidant at 600–750 °C.

regular distribution of metal ions achieved in the polyelectrolyte during the infiltration process due to the improved wettability of GDC-YSZ. This observation is consistent with an increased amount of PSC particles onto LbL-treated GDC-YSZ, as suggested by the weight changes. As a control, we performed only oxygen plasma before the infiltration to isolate the role of the polyelectrolytes. Even though the treatment improved the initial wettability of the metal precursor as observed in the reduced contact angle, it was still hard to reduce the precursor film preparation time due to the limited sites for metal ion complexation compared to LbL-assisted infiltration. Furthermore, relatively large and aggregated metal nanoparticles were covered widely over the electrode as observed in AFM and SEM images (see Figure S2 in the Supporting Information). This evidence clearly supports that the polyelectrolyte multilayer played a critical role in improving both the loading of metal precursors and fine distribution over the entire electrode through the selective complexations of metal ion precursors.

SEM images of the PSC-GDC-YSZ composite are displayed to evaluate the microstructures of the electrode (Figure 3a–e). Figure 3a shows the empty porous YSZ scaffold prior to the addition of the oxide. The appearance of the porous structure is similar to that of a sponge with the pore size ranging between 1 and 3 μm. The presence of a conformal GDC layer coating onto the porous YSZ scaffold is confirmed in Figure 3b. As shown in Figure 3c, the polyelectrolyte multilayer uniformly covers the GDC-YSZ after LbL assembly without blocking the innate porous electrode structure. After the conventional infiltration procedure followed by firing at 850 °C, PSC particles of roughly 150 nm diameter are uniformly coated on the surfaces of the GDC-YSZ scaffold (Figure 3d). Meanwhile, the microstructure of composite electrodes prepared by LbL-assisted infiltration as indicated in Figure 3e reveals more uniform coating of the PSC particles on the GDC-YSZ scaffold with a relatively smaller grain size (70 nm), probably stemming from the good wettability of the LbL procedure. This uniform coating leads to enhanced interconnection between PSC and YSZ scaffold and thus improves electrochemical performances. The electrode surface of the PSC-GDC-YSZ composite is entirely composed of electrochemical reaction sites due to the mixed ionic and electronic conducting (MIEC) property of PSC. For more concise identification of the electrochemical reaction sites for both procedures, the surface areas of each material are determined using BET measurement. It is revealed that LbL-assisted electrode presented higher surface area of 5.14 $m^2\ g^{-1}$, whereas a conventionally infiltrated electrode showed relatively lower value of 3.88 $m^2\ g^{-1}$. The higher surface area of LbL-assisted electrode could contribute to the expanded electrochemically active sites that consequently lead to the improved electrochemical performances of the material.

A scanning TEM (STEM) high-angle annular dark-field (HAADF) image of a cross-section of the PSC-GDC-YSZ composite is presented in Figure 3f, showing a 100 nm GDC film uniformly coated on the YSZ substrate and PSC particles on the GDC-YSZ layer. Elements distribution mapping images of the PSC-GDC-YSZ composite obtained by energy dispersive spectroscopy support the presence of all associated elements in the formation of the composite electrode (Figure 3g–m). On the basis of XRD, the pure PSC exhibits a single-phase perovskite structure without any impurity phase (see Figure S3 in the Supporting Information).

The temperature dependence of the electrical conductivity for the 45 wt % PSC-GDC-YSZ composite is presented in Figure 4a. Both samples show an increase in electrical conductivity with increasing temperature, representing typical

dx.doi.org/10.1021/am5048834 | ACS Appl. Mater. Interfaces 2014, 6, 17352–17357

semiconductor behavior. The electrical conductivities of PSC-GDC-YSZ composites prepared by LbL-assisted infiltration are not substantially different from that of the PSC-GDC-YSZ composite fabricated by the conventional method.

The electrocatalytic activity for the oxygen reduction reaction of PSC-GDC-YSZ composites on the YSZ electrolyte is evaluated in symmetrical cells using impedance spectroscopy. Typically, the cathodic polarization resistance normalized by the geometric electrode area, that is the area specific resistance (ASR), can be calculated from impedance spectra acquired under open circuit voltage (OCV). When the electronic conduction in the electrolyte is negligible, the cathodic polarization resistance can be adequately approximated by the diameter of the impedance loop or the difference between the high-frequency and low-frequency intercepts at the real axis. Figure 4b indicates the temperature dependence of polarization resistance for the PSC-GDC-YSZ composite electrodes via both LbL-assisted infiltration and a conventional infiltration processes. The Nyquist plots of PSC-GDC-YSZ composites at 700 °C using the two different procedures are presented in the inset of Figure 4b. The ASR values of PSC-GDC-YSZ composites at 700 °C prepared by conventional and LbL-assisted infiltrations are 0.083 and 0.054 Ω cm^2, respectively.

To study the electrochemical performance of the two types of PSC-GDC-YSZ composite electrodes in a practical fuel cell, we used electrolyte-supported cells based on a 120 μm thick YSZ electrolyte (see Figure S4 in the Supporting Information). Representative $I-V$ curves and the corresponding power densities of the cells based on these PSC-GDC-YSZ composite electrodes at various operating temperatures are shown in Figure 4c, d. The peak power densities of the cells with the composite electrodes derived from the LbL-assisted infiltration are more than 20% higher than those prepared by a studied. For example, the peak power density of the cell with an electrode prepared via traditional infiltration reached 0.098, 0.189, 0.349, and 0.604 W cm^{-2} at 600, 650, 700, and 750 °C, respectively. Under the same conditions, on the other hand, the cell with electrode derived from the LbL-assisted infiltration demonstrated peak power densities of 0.146, 0.296, 0.502, and 0.751 W cm^{-2} at 600, 650, 700, and 750 °C, as presented in Figure 4d. The observed enhancement in performance is attributed to the unique nanostructure, enlarged surface area, and increased number of active sites for electrochemical reactions of the composite electrodes derived from the LbL-assisted infiltration process.

In conclusion, we have developed a novel cathode fabrication technique for SOFCs based on an infiltration method assisted by layer-by-layer (LbL) assembly of polyelectrolytes. Preparation of the electrode with LbL-assisted infiltration not only leads to a 6.5-fold reduction in the electrode fabrication time but also ensures more uniform coating of PSC particles on the electrode. The composite electrode derived from LbL-assisted infiltration exhibits significantly enhanced electrochemical performance due to improved microstructure and increased number of active sites for electrochemical reactions. Because of the highly versatile and tunable properties of LbL assembly, we anticipate that the suggested approach will provide a new route for cost-effective electrode fabrication and microstructural enhancement for the next generation SOFCs to be operated at lower temperatures. In addition, the integration of other electroactive materials on the SOFC electrode may lead to new possibilities for the fabrication of other hybrid electrodes.

■ ASSOCIATED CONTENT

Ⓢ Supporting Information

Detailed experimental process with additional LbL growth curves, XRD, and SEM images. This material is available free of charge via the Internet at http://pubs.acs.org.

■ AUTHOR INFORMATION

Corresponding Authors

* E-mail: gtkim@unist.ac.kr.
*E-mail: bskim19@unist.ac.kr.

Author Contributions

†Y.C. and S.C. contributed equally to this work.

Notes

The authors declare no competing financial interest.

■ ACKNOWLEDGMENTS

This work was supported by a New & Renewable Energy of the Korea Institute of Energy Technology Evaluation and Planning (KETEP) grant funded by the Korea government Ministry of Trade, Industry and Energy Economy (20113020030060) and the BK21 plus (10Z2013001105) funded by the Korea government Ministry of Education.

■ REFERENCES

(1) Singhal, S. C. Advances in Solid Oxide Fuel Cell Technology. *Solid State Ionics* **2000**, *135*, 305−313.

(2) Liu, M.; Lynch, M. E.; Blinn, K.; Alamgir, F. M.; Choi, Y. Rational SOFC Material Design: New Advances and Tools. *Mater. Today* **2011**, *14*, 534−546.

(3) Steele, B. C. H. Material Science and Engineering: The Enabling Technology for the Commercialisation of Fuel Cell Systems. *J. Mater. Sci.* **2001**, *36*, 1053−1068.

(4) Wachsman, E. D.; Lee, K. T. Lowering the Temperature of Solid Oxide Fuel Cells. *Science* **2011**, *334*, 935−939.

(5) Jacobson, A. J. Materials for Solid Oxide Fuel Cells. *Chem. Mater.* **2010**, *22*, 660−674.

(6) Choi, S.; Yoo, S.; Kim, J.; Park, S.; Jun, A.; Sengodan, S.; Kim, J.; Shin, J. Y.; Jeong, H. Y.; Choi, Y.; Kim, G.; Liu, M. Highly Efficient and Robust Cathode Materials for Low-Temperature Solid Oxide Fuel Cells: $PrBa_{0.5}Sr_{0.5}Co_{22x}Fe_xO_{51d}$. *Sci. Rep.* **2013**, *3*, 2426.

(7) Minh, N. Q. Solid Oxide Fuel Cell Technology-Features and Applications. *Solid State Ionics* **2004**, *174*, 271−277.

(8) Mertens, J.; Haanappel, V. A. C.; Wedershoven, C.; Buchkremer, H. P. Sintering Behavior of $(La,Sr)MnO_3$ Type Cathodes for Planar Anode-Supported SOFCs. *J. Fuel Cell Sci. Technol.* **2006**, *3*, 415−421.

(9) Vohs, J. M.; Gorte, R. J. High-Performance SOFC Cathodes Prepared by Infiltration. *Adv. Mater.* **2009**, *21*, 943−956.

(10) Yoo, S.; Shin, J. Y.; Kim, G. Thermodynamic and Electrical Characteristics of $NdBaCo_2O_{5+\delta}$ at Various Oxidation and Reduction States. *J. Mater. Chem.* **2011**, *21*, 439−443.

(11) Choi, S.; Yoo, S.; Shin, J. Y.; Kim, G. High Performance SOFC Cathode Prepared by Infiltration of $La_{n+1}Ni_nO_{3n+1}$ (n = 1, 2, and 3) in Porous YSZ. *J. Electrochem. Soc.* **2011**, *158*, B995−B999.

(12) Park, S.; Choi, S.; Shin, J.; Kim, G. Electrochemical Investigation of Strontium Doping Effect on High Performance $Pr_{1-x}Sr_xCoO_{3-\delta}$ (x = 0.1, 0.3, 0.5, and 0.7) Cathode for Intermediate-Temperature Solid Oxide Fuel Cells. *J. Power Sources* **2012**, *210*, 172−177.

(13) Yoo, S.; Shin, J. Y.; Kim, G. Thermodynamic and Electrical Properties of Layered Perovskite $NdBaCo_{2-x}Fe_xO_{5+\delta}$-YSZ ($x$ = 0, 1) Composites for Intermediate Temperature SOFC Cathodes. *J. Electrochem. Soc.* **2011**, *158*, B632−B638.

(14) Sengodan, S.; Yeo, H. J.; Shin, J. Y.; Kim, G. Assessment of Perovskite-Type $La_{0.8}Sr_{0.2}Sc_xMn_{1-x}O_{3-\delta}$ Oxides as Anodes for Intermediate-Temperature Solid Oxide Fuel Cells Using Hydrocarbon Fuels. *J. Power Sources* **2011**, *196*, 3083−3088.

(15) Yoo, S.; Choi, S.; Shin, J.; Liu, M.; Kim, G. Electrical Properties, Thermodynamic Behavior, and Defect Analysis of $La_{n+1}Ni_nO_{3n+1+\delta}$ Infiltrated into YSZ Scaffolds as Cathodes for Intermediate-Temperature SOFCs. *RSC Adv.* **2012**, *2*, 4648−4655.
(16) Kim, G.; Vohs, J. M.; Gorte, R. J. Enhanced Reducibility of Ceria-YSZ Composites in Solid Oxide Electrodes. *J. Mater. Chem.* **2008**, *18*, 2386−2390.
(17) Lee, S.; Bevilacqua, M.; Fornasiero, P.; Vohs, J. M.; Gorte, R. J. Solid Oxide Fuel Cell Cathodes Prepared by Infiltration of $LaNi_{0.6}Fe_{0.4}O_3$ and $La_{0.91}Sr_{0.09}Ni_{0.6}Fe_{0.4}O_3$ in Porous Yttria-Stabilized Zirconia. *J. Power Sources* **2009**, *193*, 747−753.
(18) Decher, G. Fuzzy Nanoassemblies: Toward Layered Polymeric Multicomposites. *Science* **1997**, *277*, 1232−1237.
(19) Hammond, P. T. Form and Function in Multilayer Assembly: New Applications at the Nanoscale. *Adv. Mater.* **2004**, *16*, 1271−1293.
(20) Hong, J.; Han, J. Y.; Yoon, H.; Joo, P.; Lee, T.; Seo, E.; Char, K.; Kim, B. S. Carbon-Based Layer-by-Layer Nanostructures: From Films to Hollow Capsules. *Nanoscale* **2011**, *3*, 4515−4531.
(21) Skorb, E. V.; Andreeva, D. V. Layer-by-Layer Approaches for Formation of Smart Self-Healing Materials. *Polym. Chem.* **2013**, *4*, 4834−4845.
(22) Kim, B. S.; Park, S. W.; Hammond, P. T. Hydrogen-Bonding Layer-by-Layer Assembled Biodegradable Polymeric Micelles as Drug Delivery Vehicles from Surfaces. *ACS Nano* **2008**, *2*, 386−392.
(23) Lee, S. W.; Yabuuchi, N.; Gallant, B. M.; Chen, S.; Kim, B. S.; Hammond, P. T.; Shao-Horn, Y. High-Power Lithium Batteries from Functionalized Carbon-Nanotube Electrodes. *Nat. Nanotechnol.* **2010**, *5*, 531−537.
(24) Choi, Y.; Gu, M.; Park, J.; Song, H. K.; Kim, B. S. Graphene Multilayer Supported Gold Nanoparticles for Efficient Electrocatalysts Toward Methanol Oxidation. *Adv. Energy Mater.* **2012**, *2*, 1510−1518.
(25) Caruso, F.; Shi, X. Y.; Caruso, R. A.; Susha, A. Hollow Titania Spheres from Layered Precursor Deposition on Sacrificial Colloidal Core Particles. *Adv. Mater.* **2001**, *13*, 740−744.
(26) Dai, J. H.; Bruening, M. L. Catalytic Nanoparticles Formed by Reduction of Metal Ions in Multilayered Polyelectrolyte Films. *Nano Lett.* **2002**, *2*, 497−501.
(27) Kidambi, S.; Dai, J. H.; Li, J.; Bruening, M. L. Selective Hydrogenation by Pd Nanoparticles Embedded in Polyelectrolyte Multilayers. *J. Am. Chem. Soc.* **2004**, *126*, 2658−2659.
(28) Xiang, Y.; Lu, S. F.; Jiang, S. P. Layer-by-Layer Self-Assembly in the Development of Electrochemical Energy Conversion and Storage Devices from Fuel Cells to Supercapacitors. *Chem. Soc. Rev.* **2012**, *41*, 7291−7321.
(29) Ariga, K.; Yamauchi, Y.; Rydzek, G.; Ji, Q. M.; Yonamine, Y.; Wu, K. C. W.; Hill, J. P. Layer-by-Layer Nanoarchitectonics: Invention, Innovation, and Evolution. *Chem. Lett.* **2014**, *43*, 36−68.
(30) Shiratori, S. S.; Rubner, M. F. pH-Dependent Thickness Behavior of Sequentially Adsorbed Layers of Weak Polyelectrolytes. *Macromolecules* **2000**, *33*, 4213−4219.